

An improved synthesis, spectroscopic studies, FMO, MEP, Mulliken, and thermodynamic properties of 4-((E)-(4-chlorophenyl)diazenyl)-2-((E)-(2-(2-cyanoacetyl)hydrazono)methyl)phenyl methyl carbonate by DFT studies

Dr.A.Arokiasamy, Dr.S.Tamilvanan and Dr.G.Manikandan*

Department of Chemistry, Annamalai University, Annamalai nagar-608002, Tamilnadu, India

**Corresponding author: Dr. G. Manikandan (phdmani@gmail.com)*

Abstract

Theoretical analysis of the molecular structure, spectroscopic studies, and thermodynamic characteristics of the compound were done by HF and DFT-B3LYP methods using a basis set of 6-31+G(d,p). The Fourier Transform Infrared (FTIR), Nuclear Magnetic Resonance (NMR), Energy Orbitals, MEP, and Mulliken have all been investigated in great detail using quantum chemical calculations. Using optimizations and calculations based on normal coordinate force fields using density functional theory (DFT) and HF techniques with a 6-311G(d,p) basis set, the molecular structure, fundamental vibrational frequencies, and intensities of the vibrational bands were determined. The observed values and theoretical vibrational wavenumbers are compared. Charge transfer within the molecule is shown by the computed HOMO-LUMO values of -6.2056 eV and -1.2901 eV. Additionally, Mulliken calculations and the Molecular electrostatic potential (MEP) were performed. For various temperatures, the thermodynamic properties of the compound were discussed.

Keywords: *DFT, thermodynamic, FMO, MEP, Mulliken, azo*

Introduction

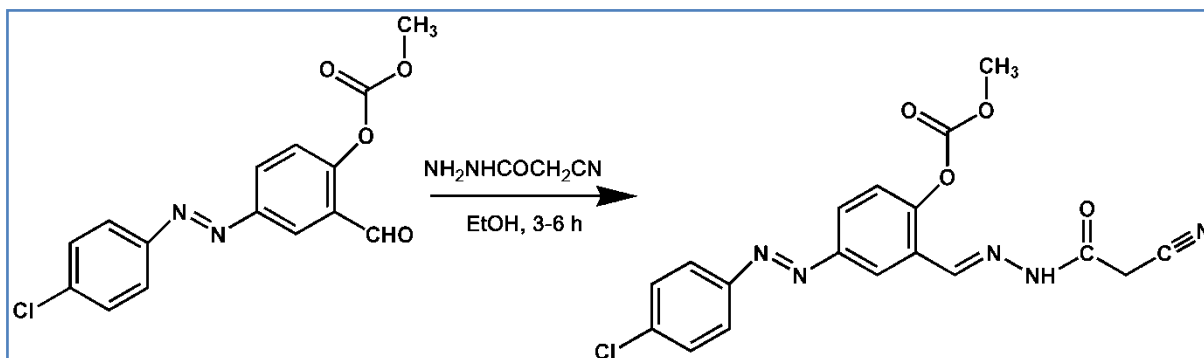
Dyes are vibrantly colored substances that are commonly used in aqueous solutions due to their high affinity for water [1, 2]. The dye's colour is primarily contributed by a chromophore group found in its chemical structure, and it is utilised in the textile, paper, leather, and food industries. Reactive dyes, azo dyes, and other synthetic dyes are used in the textile industry [3]. Azo dyes is the most common type of synthetic aromatic dye used in the textile industry for dyeing and are extremely water soluble in nature [4]. Azo dyes usually involve one, two, three, or more azo linkages, which connect phenyl and naphthyl rings and are frequently replaced with functional groups such as triazine amine, chloro, hydroxyl, methyl, nitro, and sulfonate. Monoazo dyes have one nitrogen-nitrogen bond (N=N); diazo

dyes have two N=N links; triazo dyes have three N=N bonds; and polyazo dyes have more than three N=N bonds [5, 6]. Synthetic azo dyes are recalcitrant and carcinogenic in nature for presence of –N=N– bond [7].

Experimental method

Synthesis of 4-((*E*)-(4-chlorophenyl)diazenyl)-2-((*E*)-(2-(2-cyanoacetyl)hydrazono)methyl)phenyl methyl carbonate:

For 3-6 hours, a solution of compound (*E*)-2-formyl-4-(phenyldiazenyl)phenyl methyl carbonate and cyanoacetic hydrazide in ethanol was refluxed. TLC was used to track the reaction's development. When the reaction was finished, the solid product separated on cooling, was collected by filtering, and was thoroughly washed with water. The recrystallization of a 1:1 combination of ethanol and ethyl acetate resulted in a pure sample [8]. (**Scheme 1**). Brownish yellow colour solid, mp: 218-220 °C, Chemical Formula: C₁₈H₁₄ClN₅O₄, **Elemental Analysis:** Obtained - C (54.12 %), H (3.71 %), N (17.64%), calculated - C (54.08 %), H (3.53%), N (17.52%). **FT-IR (KBr) (cm⁻¹):** 3446 (N-H), 2849-3103 (C-H), 1750 (C=O, carbonate), 1738 (C=N, hydrazones), 2231 (C≡N), 1654 (-C=N), 1498 (-N=N-), 1022 and 1195 (-C-O-C-).



Scheme 1

Computational methodology

All calculations were carried out using the Gaussian 09 software package [9]. Theoretical calculations in the gas phase were used to optimize the 4-((*E*)-(4-chlorophenyl)diazenyl)-2-((*E*)-(2-(2-cyanoacetyl)hydrazono)methyl)phenyl methyl carbonate, such as thr HF and DFT-B3LYP methods, using a basis set of 6-31+G(d,p). NMR chemical shifts (reference TMS) were calculated using the Gauge-Invariant Atomic Orbital (GIAO) technique for the HF and DFT-B3LYP/6-31+G (d, p) levels. The same level of theory was used to calculate the HOMO-LUMO energy gap, global chemical reactivity descriptors, the molecule electrostatic potential, and Mulliken atomic charges.

Results and Discussion.

Infrared and NMR Analysis

According to the outcomes of the vibrational investigation, the molecule has 42 atoms with C1 symmetry and 120 normal vibrational modes. There are 120 vibrational modes in a compound, which are divided up into 43 stretching, 38 bending, 32 torsion, and 7 out-of-plane modes. Figure 1 displays combined experimental and theoretical FT-IR spectra. Depending on certain studies, the carbonyl stretching vibrations should occur between 1715 and 1680 cm^{-1} . In our case, the experimental FT-IR identified the carbonate's C=O stretching band at 1767 and 1763 cm^{-1} .

The ^1H and ^{13}C chemical shifts of the molecule were computed using the HF and DFT-B3LYP methods with a 6-31+G(d, p) basis set. Table 1 shows experimental and computational chemical shift results, as shown in Fig 2. Two signals were observed in the upfield region of the experimental ^1H NMR spectrum, one at 3.949 (s) ppm with three protons integral, which corresponds to H27, H28, and H29 atoms, and another at 4.077 with protons integral, which corresponds to the H39 atom. Aromatic carbons' ^{13}C NMR spectrum signals are detected at 122.4, 124, 126.6, 138.9, 149.6, and 150.1 ppm, respectively. The shielded signals recorded at 24.01 and 55.54 ppm are attributed to C37 (methylene) and C27 (carbonate methyl carbon).

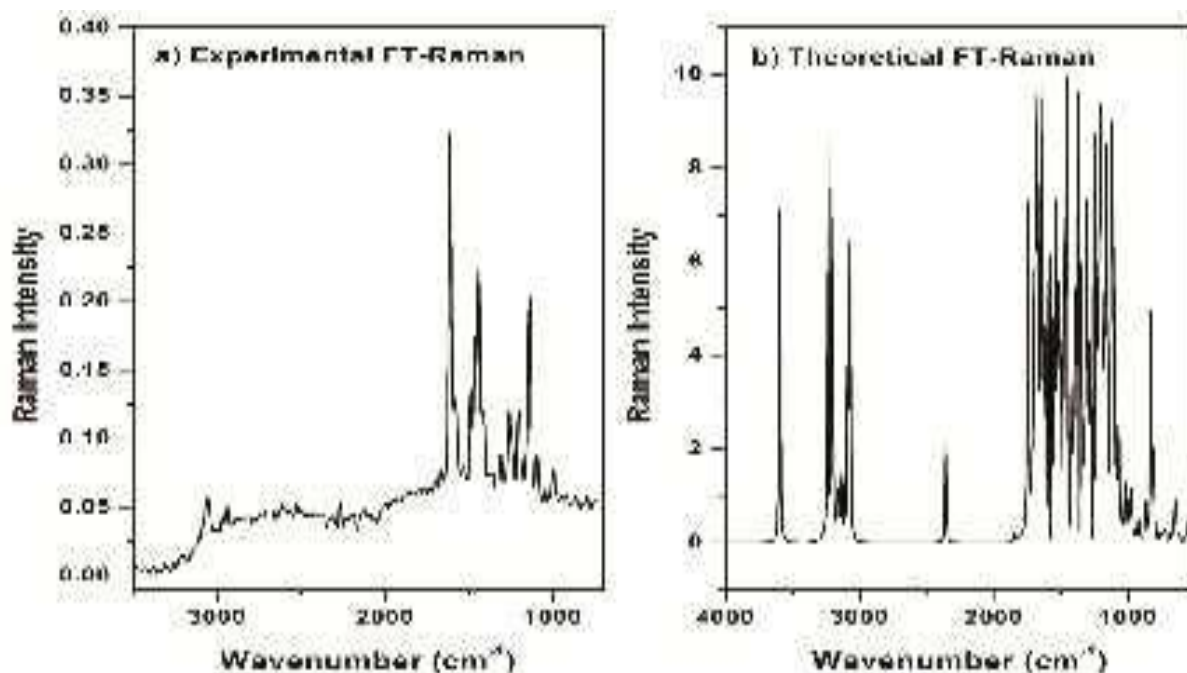
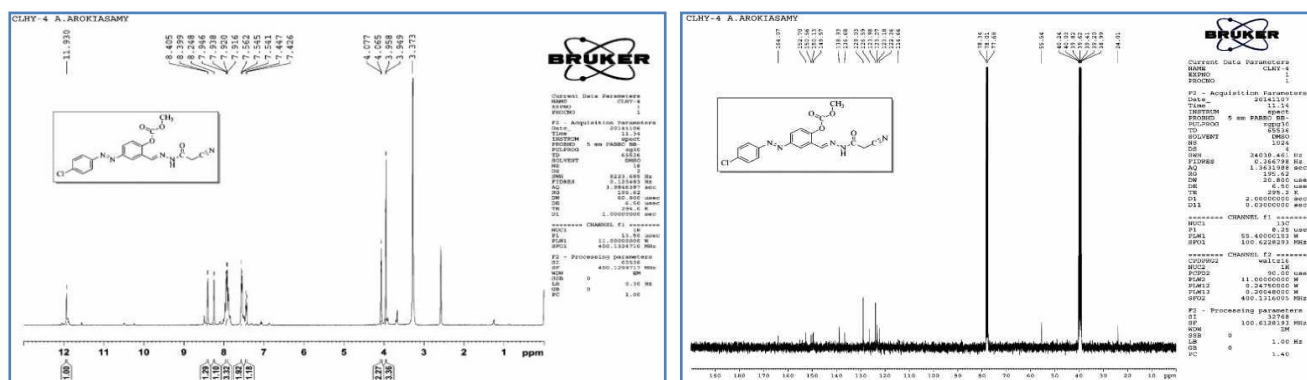


Fig. 1. Experimental and simulated FT-IR spectra of compound

Fig. 2. Experimental ^1H and ^{13}C NMR spectra of compoundTable 1. Experimental and calculated ^1H and ^{13}C chemical shift (ppm) values of compound

Atom	HF	DFT	Expt.	Atom	HF	DFT	Expt
H7	8.595	7.075	7.541	C3	119.5	123	129
H8	9.24	7.74	7.938	C4	154.6	156.8	150.6
H9	9.231	7.73	7.938	C5	139.8	142.5	129
H10	8.754	7.239	7.562	C6	133.5	136.5	123.3
H17	9.199	7.697	7.946	C13	155.2	157.3	150.1
H19	9.455	7.962	8.399	C14	143.6	146.2	138.9
H21	8.486	6.961	7.426	C15	122.8	126.2	126.6
H27	4.636	2.994	3.949	C16	132.7	135.7	122.4
H28	4.702	3.062	3.949	C18	130.2	133.3	124
H29	4.86	3.225	3.949	C20	157.8	159.8	149.6
H31	9.381	7.885	8.248	C23	155.5	157.6	152.7
H34	9.145	7.643	11.93	C26	64.33	69.97	55.54
H38	4.451	2.803	4.065	C30	161.4	163.3	123.2
H39	4.863	3.228	4.077	C35	162.9	164.7	164.1
C1	153	155.2	136.7	C37	34.04	40.85	24.01
C2	133.4	136.4	123.3	C40	115	118.7	114.7

Molecular geometry

The molecular structural properties of the compound, such as bond lengths, bond angles, and dihedral angles, were computed using the HF and DFT-B3LYP techniques using a 6-31+G(d, p) base set and listed in Table 3. The computed structural characteristics were compared to the crystal structures of azo compounds found in the literature. The variations in the C–C and C–N bond length values by HF and DFT- B3LYP method with the corresponding literature values of compound are C1C2 (1.389/1.401/1.393 Å), C1C6 (1.381/1.395/1.398 Å), C4N11 (1.42/1.416/1.428 Å), N12C13 (1.42/1.417/1.425 Å), Similar

variations in C-C-N, C-N-N, and C-C-H bond angles can be ascribed to substituent effect, electro negativity, and the presence of a lone pair of electrons in the molecule, as in the case of C₃C₂H₇ (120.5°/120.7°/118.8), C₄C₅H₉ (119.1°/118.7°/119.2), C₆C₅H₉ (120.4°/120.7°/121.0), N However, it was observed that the computed C-H and C-C bond lengths of phenyl rings were in good agreement with the relevant literature values within 0.01-0.02. [10]. The dihedral angles of C₂C₁C₆H₁₀ (179.9/180°) and N₁₁N₁₂C₁₃C₁₄ (178.1/179.7/176°), which deviate from the planar angles (0° or 180°), confirm that the carbonate and hydrazone groups are located on the upper side of the molecular plane because they both have the same sign, and the (phenyl diazenyl)phenyl group is in the same plane as is shown in Fig.3.

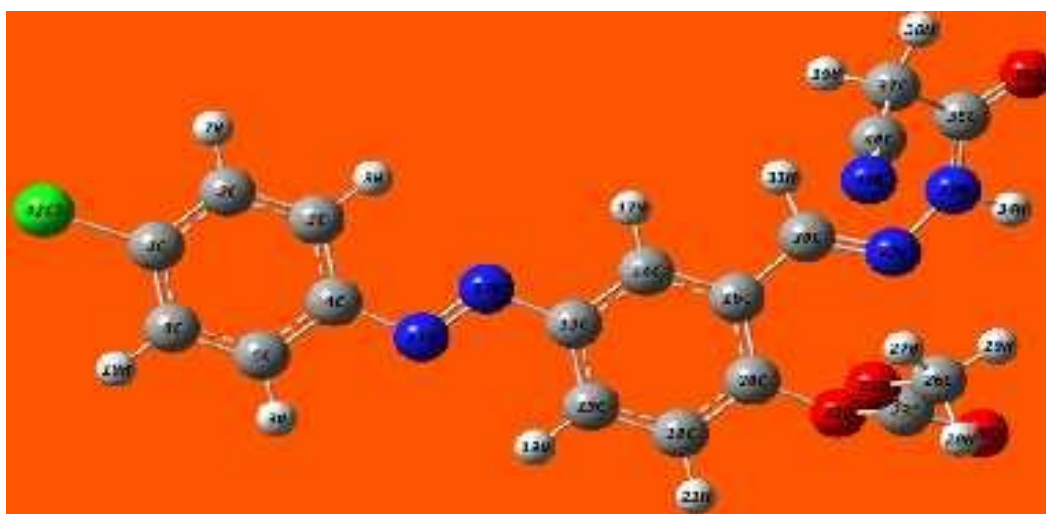


Fig.3. Optimized molecular structure of the complex

Table 2. HOMO- LUMO energies and calculated global reactivity parameters of compound

Energy	Compound	
	HF [eV]	DFT [eV]
EHOMO	-8.8439	-8.192
ELUMO	0.8431	-5.7549
ΔE_1	9.687	2.4383
EHOMO-1	-9.4187	-8.464
ELUMO+1	1.395	-5.326
ΔE_2	8.0237	3.139
I_p	8.8439	8.192
A	0.8431	5.7549
η	4.0004	1.2186
χ	4.8435	6.9735
σ	0.25	0.8206
ω	1.9781	0.1835

HOMO-LUMO analysis

The terms HOMO and LUMO refer to a molecule's ionisation potential and electron affinity, respectively. The HOMOLUMO energy gap provides the electron-donating, accepting, and stability properties of the molecule [11]. Figure 4 displays a graphical depiction of HOMO and LUMO. Calculations are performed for the title compound's other significant properties, including its ionisation potential, electron affinity, electronegativity, chemical potential, chemical hardness, chemical softness, and electrophilicity index. Table 5 lists the aforementioned characteristics. According to this table, the energy gap between the HOMO and LUMO orbitals is 2.4383 eV, with the HOMO orbital having a lot of electrons with an energy of -8.192 eV and the latter orbital having less electrons with an energy of -5.7549 eV. This bandgap indicates that the title compound is highly stable, that internal charge transfer occurs, and that it has a bioactive character [12, 13]. Koopman's theorem states that IP and EA are connected to the HOMO ($IP = -E_{HOMO}$ (8.192 eV)) and LUMO ($EA = -E_{LUMO}$ (5.7549 eV)) energies, respectively. Mulliken defined as $\chi [= -1/2 (E_{HOMO} + E_{LUMO})$ (6.9735 eV)], and this variable symbolises the attraction of electrons caused by the interactions of an atom and a functional group, which causes the electronic charges to move from areas of low to high electronegativity inside a molecule. Figure 4 and Table 2 illustrate the computed values ($\omega = \mu^2/2\eta$ eV (0.1835 eV), which were determined by Maynard et al. [14] and Parr et al. [15].

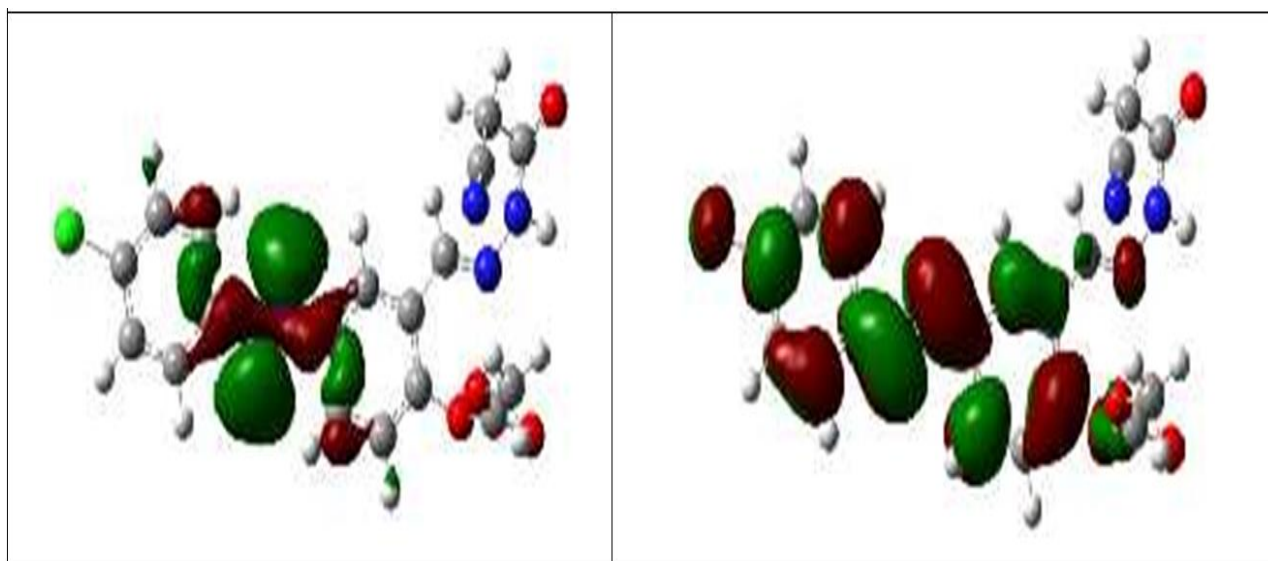


Fig.4. Frontier molecular orbitals molecular HOMO and LUMO of compound

Table 3. Optimized geometrical parameters (bond length, bond angle and Dihedral Angles) of compound

Bond distances (Å)			Bond angles (°)			Dihedral angles (°)		
	HF	DFT		HF	DFT		HF	DFT
C1C2	1.389	1.401	C2C1C6	121.2	121.3	C6C1C2C3	0.20	0.03
C1C6	1.381	1.395	C2C1C142	119.3	119.2	C6C1C2H7	-180	-180
C1C142	1.741	1.754	C6C1C142	119.5	119.5	C142C1C2C3	-180	-180
C4N11	1.420	1.416	C1C2C3	119.6	119.5	C142C1C2H7	0.19	0.03
N11N12	1.218	1.259	C1C2H7	120.0	119.8	C2C1C6C5	-0.03	-0.01
N12C13	1.420	1.417	C3C2H7	120.5	120.7	C2C1C6H10	179.9	180
O22C23	1.333	1.367	C4C5C6	120.5	120.6	C142C1C6H10	0.01	0.01
C23O24	1.182	1.203	C4C5H9	119.1	118.7	N11C4C5C6	-180	-180
C23O25	1.31	1.336	C6C5H9	120.4	120.7	N11C4C5H9	-0.08	0.00
O25C26	1.426	1.446	C1C6C5	119.0	118.9	H9C5C6H10	-0.07	0.00
N32N33	1.354	1.39	N11N12C13	115.8	115.0	C4N11N12C13	179.7	179.9
N33H34	1.000	1.014	N12C13C14	115.6	115.5	N11N12C13C14	178.3	179.7
N33C35	1.356	1.378	N12C13C15	124.2	125.1	N11N12C13C15	-1.72	0.15
C37H38	1.081	1.093	O22C23O24	121.1	121.3	N12C13C14C16	179.9	179.8
C37H39	1.083	1.094	O22C23O25	112.8	111.3	N12C13C14H17	0.17	-0.25
C37C40	1.470	1.464	O24C23O25	126.1	127.3	N12C13C15C18	-180	179.8
C40N41	1.135	1.161	O25C26H27	105.3	105.1	N12C13C15H19	0.55	0.03

Molecular electrostatic potential (MEP) maps

MEP, which would be associated with electronic density and their interactions, is a very useful measure for determining locations where electrophilic and nucleophilic reactions may occur. A colour system was used to distinguish between regions with maximum potential for the negative, maximum potential for the positive, and the potential areas between them. The red colour symbolises negative electrostatic potential, a surface for electrophilic attacks, whereas the blue colour represents positive electrostatic potential, a surface for nucleophilic attacks. Colors like yellow, green, and orange are used to illustrate the areas between negative and positive potentials. Potential increases in the order red < orange < yellow < green < blue [16]. As seen in O23, O25, O37, and N41 in Figure 5, the red area denotes the highest electrostatically negative potential. The green zone denotes zero potential, whereas the blue region, which is the positive region, is mostly centred on hydrazide -NH- and -CH2- groups that are favourable for nucleophilic attack.

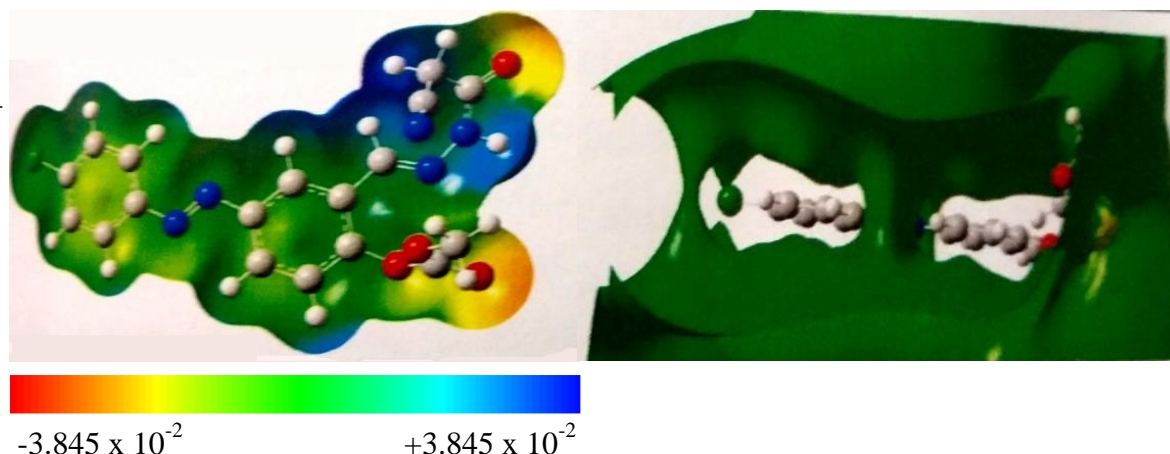


Fig. 5. Molecular electrostatic potential of compound

Mulliken atomic charge

The Mulliken population study [17] provides the atomic charge density or orbital density on individual atoms derived using DFT-B3LYP levels with a basis set of 6-31+G(d, p), and the values of compound is presented in Table 4. Figure 6 depicts the net Mulliken atomic charge of atoms in a compound. In phenyl (1), the Mulliken atomic charges of C2, C4, and C6 atoms were found to be negative, whereas C1, C3, and C5 atoms exhibited positive charges. Carbon atoms C13, C14, and C18 were found to be negatively charged (phenyl (2) rings), whereas C15, C16, and C20 atoms showed positive charges, with C13 having the highest negative value. The magnitude of the carbon (C4) atom bonded to the nitrogen atom with the highest negative charge, i.e., it acted as an electron acceptor, whereas the largest accumulation of positive charge was determined to be on carbon atom C15. Because of the substituent effect, the C1 carbon atom acted as an electron donor.

Table 4. Mulliken atomic charges of compound

Atoms	charges	Atoms	charges	Atoms	charges
C1	0.19	C15	0.767	H29	0.163
C2	-0.326	C16	0.767	C30	-0.281
C3	0.605	H17	0.129	H31	0.105
C4	-1.349	C18	-0.07	N32	-0.093
C5	0.439	H19	0.157	N33	-0.227
C6	-0.463	C20	0.109	H34	0.344
H7	0.15	H21	0.15	C35	0.232
H8	0.152	O22	-0.331	O36	-0.389
H9	0.141	C23	0.574	C37	-0.01
H10	0.151	O24	-0.442	H38	0.23
N11	0.032	O25	-0.251	H39	0.2
N12	-0.014	C26	-0.15	C40	0.167
C13	-1.138	H27	0.173	N41	-0.42
C14	-0.594	H28	0.156	C142	0.27

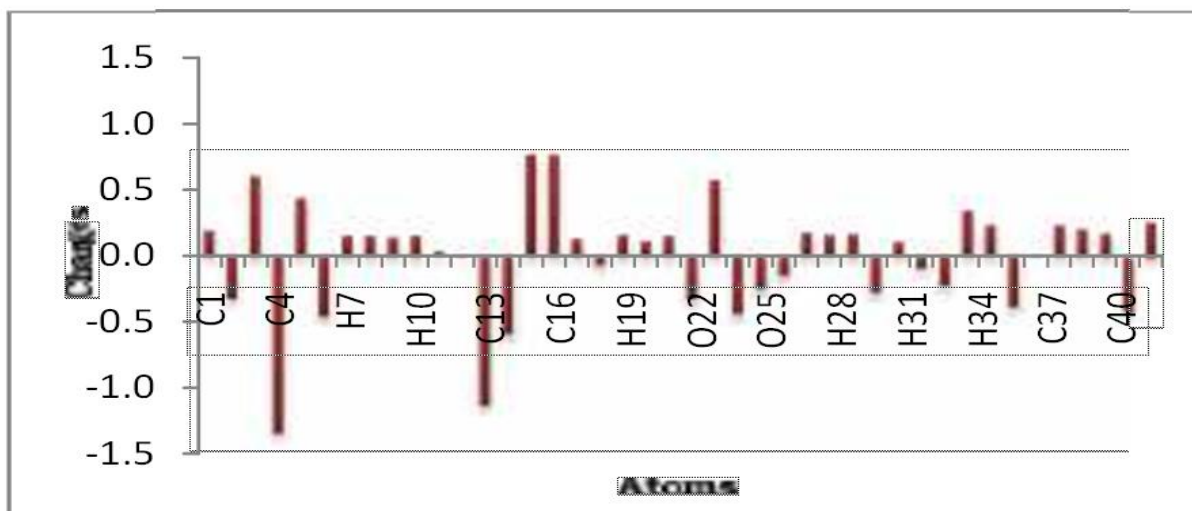


Fig. 6. Mulliken atomic charges of compound

Thermodynamic properties

On the basis of translational, rotational, vibrational, and electronic energies. At 298.15 K and 1 atm of pressure, the statistical thermochemical analysis was performed. This resulted from the molecular vibration becoming more prominent as the temperature increased. The temperature dependence of the thermodynamic properties of heat capacity ($C^{\circ}p$), entropy ($S^{\circ}m$) and zero-point vibrational energy were also determined by HF and B3LYP levels with a 6-31+G(d, p) basis set [18,19] and the values of the compound. From the results as shown in the Table 5, the total thermal energies of compound in HF method is higher than DFT-B3LYP method. The corresponding fitting equations are $S^{\circ}m = 224.89507+0.71864T-1.78038E-4T^2$ and $C^{\circ}p = 11.25858+0.65935T-2.95072E-4T^2$.

Table 5. Calculated thermodynamic parameters of compound

Parameters	Compound	
	HF	DFT
SCF energy [a.u.]	-1721	-1729.2
Total thermal energies [kcal/mol]	220.54	206.15
Zero point energy [kcal/mol]	204.97	189.71
Rotational constants [GHz]	-	
X	0.1891	0.3126
Y	0.0676	0.0562
Z	0.0521	0.0507
Entropy [cal/mol.K]	184.7	185.78
Heat capacity [cal/mol.K]	88.55	94.8

Conclusion

In the present work, quantum computational and spectroscopic analysis of the title compound was carried out using HF and DFT (B3LYP/6-311G(d,p) methods. Bond lengths, bond angles, and dihedral angles of molecular geometry parameters, show good agreement with experimental data. The title compound was exposed to spectroscopic analyses using FTIR, NMR, and theoretical values derived using B3LYP techniques using basis set were compared with the experimental results. The calculated energy gap between HOMO and LUMO was 2.4383 eV indicates that the compound is incredibly stable and that charge transfer occurs within the molecule. Physicochemical characteristics, quantum chemical parameters, and the frontier molecular orbital analysis have all been predicted using the same level in gas phase theory. In according to the MEP diagrams, the highest electrostatically negative potential is shown by the red region, as seen in O23, O25, O37, and N41. The Mulliken charge analysis interprets the alteration of chemical and physical properties while describing the redistribution of electrons (charges). The compound's thermodynamic properties and parameters have been calculated.

References

- [1] M. Sudha, A. Saranya, G. Selvakumar, *et al*, Microbial degradation of azo dyes: a review. *Int J Curr Microbiol App Sci* 3(2), (2014) 670–690.
- [2] B.E. Barragán, C. Costa, M.C. Marquez, Biodegradation of azo dyes by bacteria inoculated on solid media. *Dyes Pigments* 75(1), (2007) 73–81.
- [3] J. Bell, JJ. Plumb, CA. Buckley, *et al*, Treatment and decolorization of dyes in an anaerobic baffled reactor. *J Environ Eng* 126(11), (2000)1026–1032.
- [4] RG. Saratale, GD. Saratale, JS. Chang, *et al*, Bacterial decolorization and degradation of azo dyes: a review. *J Taiwan Inst Chem Eng* 42(1) (2011) 138–157.
- [5] A. Baban, A. Yediler, D. Lienert *et al*, Ozonation of high strength segregated effluents from a woollen textile dyeing and finishing plant. *Dyes Pigments* 58(2), (2003) 93–98.
- [6] SK. Sen, S. Raut, P. Bandyopadhyay *et al*, Fungal decolouration and degradation of azo dyes: a review. *Fungal Biology Reviews* 30(3) (2016) 112–133.
- [7] N. Puvaneswari, J.Muthukrishnan, P. Gunasekaran, Toxicity assessment and microbial degradation of azo dyes 44(8), (2006):618-626.

- [8] M. Odabasoglu, C. Albayrak, R. Ozkanca, F.Z. Aykan, P. Lonecke, Some polyhydroxy azoazomethine derivatives of salicylaldehyde: synthesis, characterization, spectroscopic, molecular structure and antimicrobial activity studies, *J. Mol. Struct.* 840 (2007) 71–89.
- [9] M.J. Frisch, G.W. Trucks, D.J. Fox, Gaussian 09, Revision E.01, Gaussian, Inc., Wallingford CT, 2009.
- [10] A.U. Khan, F.Avecillia, N.Malik, Md. Shahid Khan, Md. Mushtaque, *J. Mol. Struct.* 1122, (2016) 100-110.
- [11] S. Renuga, M. Karthikesan, S. Muthu, FTIR and Raman spectra, electronic spectra and normal coordinate analysis of N, N-dimethyl-3-phenyl-3-pyridin-2-yl-propan-1- amine by DFT method, *Spectrochim. Acta Mol. Biomol. Spectrosc.* 127 (2014) 439–453.
- [12] Y.S. Mary, C.Y. Panicker, M. Sapnakumari, B. Narayana, B.K. Sarojini, A.A. Al-Saadi, C. VanAlsenoy, J.A. War, FT-IR, NBO, HOMO-LUMO, MEP analysis and molecular docking study of 1-[3-(4-fluorophenyl)-5-phenyl-4,5-dihydro-1H-pyrazol-1-yl]ethanone, *Spectrochim. Acta* 136 (2015) 483–493.
- [13] D. Chen, H. Wang, HOMO-LUMO energy splitting in polycyclic aromatic hydrocarbons and their derivatives, *Proc. Combust. Inst.* 37 (2019) 953–959.
- [14] A.T. Maynard, M. Huang, W.G. Rice, D.G. Covell, Reactivity of the HIV-1 nucleocapsid protein p7 zinc finger domains from the perspective of density-functional theory, *Proceedings of the National Academy of Sciences.* 95 (1998) 11578–11583.
- [15] R.G. Parr, C. Hill, N. Carolina, Electrophilicity Index, *Journal of the American Chemical Society.* 121 (1999) 1922–1924.
- [16] D.A. Zainuri, S. Arshad, N.C. Khalib, Experimental and theoretical spectroscopic and structural analyses of a new chalcone single crystal derived from 4-bromo-2-thiophenecarboxaldehyde, *Molecular Crystals and Liquid Crystals.* 650 (2017) 87–101.
- [17] R.S. Mulliken, A New Electroaffinity Scale ; Together with Data on Valence States and on Valence Ionization Potentials and Electron Affinities, *The Journal of Chemical Physics.* 2 (1934) 782–793.
- [18] J.B. Ott, J.B. Goates, *Chemical Thermodynamics: Principles and Applications*, Academic Press, San Diego, 2000.
- [19] N. Issaoui, S. M.H. Ghalla, Molecular structure, vibrational spectra, AIM, HOMO-LUMO, NBO, UV, first order hyperpolarizability, analysis of 3-thiophenecarboxylic acid monomer and dimer by Hartree-Fock and DFT theory, *Spectrochim. Acta Mol. Biomol. Spectrosc.* 136 (2015) 1227–1242.